Motional Dynamics of the Catalytic Loop in OMP Synthase †

ARTICLE *in* BIOCHEMISTRY · FEBRUARY 1999

Impact Factor: 3.02 · DOI: 10.1021/bi982057s · Source: PubMed

5 AUTHORS, INCLUDING:

Gary Wang
University of Florida
26 PUBLICATIONS **2,342** CITATIONS
SEE PROFILE

Sean Cahill
Albert Einstein College of Medicine
59 PUBLICATIONS **1,724** CITATIONS
SEE PROFILE

Motional Dynamics of the Catalytic Loop in OMP Synthase[†]

Gary P. Wang,[‡] Sean M. Cahill,[§] Xiaohong Liu,[§,||] Mark E. Girvin,*[,§,⊥] and Charles Grubmeyer*[,‡]

Fels Institute for Cancer Research and Molecular Biology, and Department of Biochemistry, Temple University School of Medicine, 3307 North Broad Street, Phildelphia, Pennsylvania 19140, and Department of Biochemistry, Albert Einstein College of Medicine, 1300 Morris Park Avenue, Bronx, New York 10461

Received August 25, 1998

ABSTRACT: In de novo pyrimidine biosynthesis, orotate phosphoribosyltransferase catalyzes the formation of orotidine 5′-monophosphate (OMP) from orotic acid and α-D-5-phosphoribosyl-1-pyrophosphate (PRPP). The known three-dimensional structure of the dimeric enzyme from *Salmonella typhimurium* is similar to that of other Type I phosphoribosyltransferases (nucleotide synthases) with a solvent-exposed active site atop a Rossman-type nucleotide binding fold. The three-dimensional structure of an enzyme−inhibitor complex [Henriksen et al. (1996) *Biochemistry 35,* 3803−3809] indicates that one of the two identical solvent-exposed loops can descend to cover the active site of the adjacent subunit of the dimeric enzyme. Catalytically essential residues are known to reside on this loop. In the present work, sensitivity toward limited proteolysis by trypsin confirms that the loop is solvent-exposed. Protection by PRPP and, to a lesser extent, by OMP demonstrates the existence of a second, trypsin-inaccessible, loop position. Two-dimensional ^{1}H-^{15}N NMR relaxation experiments on [α-^{15}N]histidine-labeled WT OPRTase yielded backbone ^{15}N T_1 and T_2 relaxation times and $^{15}N\{^{1}H\}$ NOE for His-105 (a loop residue) that are characteristic of small peptides. These results document that the surface loop is highly flexible in the unliganded enzyme. Addition of a hydrolytically stable PRPP analogue to the enzyme resulted in a significant reduction of His-105 peak intensity, indicating a dramatic change in the dynamic properties of the loop backbone in the analogue-ligated enzyme. ^{1}H NMR titrations on histidine C2 protons, coupled with ^{1}H and ^{31}P titrations monitoring the C1H and 5-phosphate PRPP resonances, allowed the quantitation of the rates of loop movement during product release, and relate protein motion to enzymatic catalysis. These results suggest that loop opening and PRPP release is a two-step process, whose overall rate is partially rate-limiting in the reverse pyrophosphorolysis reaction.

Mobile peptide loops have increasingly been recognized as being important in enzymatic catalysis. Understanding their dynamics is central to our knowledge of coupling between movement and catalysis. Functionally, loop motions have been suggested to be necessary for recruiting essential residues for enzymatic catalysis and/or protecting reactive intermediates from solvolysis (*1*). The roles and the time scales of loop movements have recently been delineated in several enzymes. The flexible loop (loop 1) of dihydrofolate reductase, for example, exchanges between two conformations with a rate constant (35 s^{-1}) comparable to that for enzymatic catalysis (*2*); closure of the loop over the active site is believed to contribute to transition-state stabilization during catalysis (*3, 4*). Loop closure in triosephosphate isomerase, also occurring on the time scale of enzyme turnover (*5*), stabilizes the enediol phosphate intermediate and prevents an alternative phosphate elimination reaction (*6*).

Very little is known about the relationship between ligation states of enzymes and rates of loop movement. Two general models describe loop motions in response to ligand binding: the ligand-gated model, in which binding of ligand precipitates the closure of a loop, and the equilibrium model, in which a loop equilibrates between its open and closed forms and site occupancy by the bound ligand may stabilize a closed conformation. Although loop motions in proteins have frequently been assumed to be ligand-gated, owing heavily to the wide acceptance of the induced-fit mechanism (*7*), recent studies on triosephosphate isomerase (*5*) and protein tyrosine phosphatases (*8*) indicate that loop movements may in fact be ligand-independent, thus favoring equilibrium models.

Structurally, movements of protein loops can be classified into two major types. In rigid-body motion, a structured element undergoes rotational and/or translational motion, usually about a hinge, without substantial internal reordering (*9*). At the other extreme, a structured or flexible element moves to adopt a new stable structure. Both rigid-body and flexible loop movements are commonly seen among mobile elements. Although the former is conceptually simpler, the reordering movement is both abundant and important. The nature of loop movement in proteins has recently been explored using X-ray crystallography (reviewed by ref *9*), nuclear magnetic resonance, and molecular dynamics simula-

[†] Supported by NIH (GM48623).

* To whom reprint request should be addressed. Phone: (215) 707-4495. Fax: (215) 707-5529. E-mail: ctg@ariel.fels.temple.edu.

[‡] Temple University School of Medicine.

[§] Albert Einstein College of Medicine.

[||] Current address: Department 155, Bristol-Myers Squibb Company, 5 Research Parkway, Wallingford, CT 06492-7660.

[⊥] Phone: (718) 430-2025. Fax: (718) 430-8565. E-mail: girvin@aecom.yu.edu.

10.1021/bi982057s CCC: $18.00
Published on Web 12/12/1998

tions. For example, the crystal structures of pancreatic α-amylase showed ordering of an unstructured surface flexible loop upon binding a substrate analogue (*10*). Transferred nuclear Overhauser effect studies on peptides of the GroES mobile loop indicated that the disordered loop peptide adopts a hairpin turn upon binding to GroEL (*11*, *12*). In the solution NMR structure of ribosomal protein L11, RNA binding results in restructuring of a disordered mobile loop (*13*). In triosephosphate isomerase, however, molecular dynamics simulations and X-ray crystallographic studies have suggested that a catalytically essential mobile loop opens and closes the active site in a rigid-body type motion with hinges at both ends of the peptide loop (*14*−*16*).

Orotate phosphoribosyltransferase (OPRTase)[1] or OMP synthase, a de novo pyrimidine biosynthetic enzyme, catalyzes a magnesium ion-dependent group transfer reaction in which the phosphoribosyl moiety of α-D-5-phosphoribosyl 1-pyrophosphate (PRPP) is reversibly transferred to orotate to generate orotidine 5′-monophosphate (OMP) and pyrophosphate. Kinetic isotope effects studies (*17*) indicate that the OPRTase reaction proceeds through an expanded transition state of high oxocarbenium character with low bond orders to attacking orotate and leaving pyrophosphate. Stabilization of these S_N1-like transition states on an enzyme requires not only optimal electrostatic and hydrogen bonding interaction between catalytic groups and transition states but also exclusion of adventitious nucleophiles such as water to prevent solvolysis. However, examination of the two available structures of liganded *Salmonella typhimurium* OPRTase (*18*, *19*) revealed an active site that is largely solvent-exposed, suggesting that an enzyme conformation change must occur during substrate turnover to shield the developing transition state from bulk solvent. Adjacent to the active site and projecting into the solution is a highly conserved loop (residues 99-RKEAKDHGEGG-109) whose poor electron density suggests high flexibility and which could potentially serve as a lid to close the active site. The amino acid sequence of the loop constitutes the region of highest conservation in the protein among the two dozen OPRTases of known primary structure. This conservation is inconsistent with its solvent-extended and disordered position in nearly all known three-dimensional structures. On the basis of the proposed transition-state structure, sequence conservation, and the catalytic importance of loop residues Arg-99 (unpublished results; this lab), Lys-100, and Lys-103 (*20*), we have postulated (*20*, *21*) that the flexible loop descends during catalysis from its solvent-extended intersubunit position to occlude the active site. We have previously shown using in vitro complementation that catalysis in one active site of the dimeric OPRTase requires a contribution from the flexible loop of the adjacent subunit (*21*), a strong indication that closure of the flexible loop occurs across the dimer interface.

There are now several Type I PRTase (*22*) three-dimensional structures that show homologous flexible loops in loop-closed conformations (*23*−*25*). The highly identical crystalline *Escherichia coli* OPRTase with bound inhibitory sulfate anion (*23*) forms an asymmetric dimer with sulfate in both active sites, but with one of the two flexible loops adopting a loop-down conformation and one loop remaining in a flexible solvent-exposed position. As predicted, the loop in the down conformation is positioned over the active site of the adjacent subunit, allowing the critical loop residue Lys-103 to interact with bound sulfate. In the unliganded hypoxanthine-guanine-xanthine phosphoribosyltransferase (HGXPRTase; ref *24*), the unoccupied active site is partially occluded by its catalytically essential (*26*) peptide loop. The most revealing loop-down structure of a PRTase, that of glutamine PRPP amidotransferase (GPATase) in complex with a nonproductive PRPP analogue, shows reordering of the flexible loop structure upon its closure over the active site, forming a nascent solvent-occluded tunnel for the attacking ammonia nucleophile (*25*). Although the necessity of active site closure by flexible loops in PRTases has become appreciated, the dynamics and the catalytic contributions of the flexible loops remain largely unexplored.

In the accompanying paper (*27*), we have shown that a slow physical step following group transfer chemistry limits the overall catalytic rate of *S. typhimurium* OPRTase. In this paper, we have utilized proteolysis studies and NMR spectroscopy to characterize loop dynamics. Proteolysis results support our hypothesis that ligand binding is coupled to flexible loop motion. Two-dimensional ^1H-^{15}N heteronuclear NMR relaxation experiments clearly indicate that the surface loop is highly flexible in solution. NMR titrations with PRPP and sulfate have allowed us to construct a model which identifies loop opening as partially rate-limiting during enzymatic catalysis.

EXPERIMENTAL PROCEDURES

Materials. Mutagenic primers were synthesized at Ransom Hill Bioscience, Inc. Materials for mutagenesis and DNA sequencing procedures were purchased from U. S. Biochemicals and New England Biolabs Inc. DTT was from U. S. Biochemicals. Buffers, orotic acid, PRPP, OMP, amino acids, other reagent grade biochemicals, and bacterial culture media were obtained from Sigma. TFA was purchased from Fisher. Sephadex G-50 resin was from Pharmacia. [α-^{15}N]Histidine and [α-^{15}N]leucine were synthesized at Cambridge Isotope Labs. D_2O (99.9 atom % D) was from Aldrich. SYPRO Orange protein gel stain and protein molecular weight standards were from Molecular Probes.

Proteolysis of WT and K26A Mutant OPRTase. A 1 mL reaction mixture containing 0.5 mg/mL WT or K26A OPRTase, 10 mM $CaCl_2$, and 6 mM $MgCl_2$ in 75 mM sodium Tricine at pH 8.5 was incubated in a 30 °C dry bath for 10 min, followed by the addition of trypsin (0.05 mg/mL; Worthington TPCK-treated) to initiate proteolytic digestion. Samples (100 μL) were removed at 5 min intervals and quenched in 1 mM phenylmethanesulfonyl fluoride (PMSF). For ligand protection experiments, 2 mM PRPP or 100 μM

[1] Abbreviations: DTT, dithiothreitol; EDTA, ethylenediaminetetraacetic acid, GPATase, glutamine phosphoribosylpyrophosphate amidotransferase; HSQC, heteronuclear single quantum coherence; IPTG, isopropyl D-thiogalactopyranoside; LB, Luria broth; NMR, nuclear magnetic resonance; OMP, orotidine 5′-monophosphate; OPRTase, orotate phosphoribosyltransferase; PIPES, piperazine-*N*,*N*′-bis(2-ethanesulfonic acid sesquisodium salt); PCR, polymerase chain reaction; PMSF, phenylmethylsulfonyl fluoride; PP_i, inorganic pyrophosphate; PRPNP, α-D-5-phosphoribosyl-1-imidodiphosphate; PRPP, α-D-5-phosphoribosyl-1-pyrophosphate; PRTase, phosphoribosyltransferase; SDS−PAGE, sodium dodecyl sulfate−polyacrylamide gel electrophoresis; TFA, trifluoroacetic acid; Tris, Tris(hydroxymethyl)aminomethane; WT, wild-type OPRTase.

OMP was included for WT trypsinolysis; 2 mM PRPP or 1 mM OMP was used for K26A trypsinolysis. Each PMSF-quenched sample was assayed in the reverse pyrophosphorolysis reaction using the standard enzymatic assay described below, and the cleavage products were analyzed by 15% SDS−PAGE (*28*). SDS gels were stained with SYPRO Orange protein gel stain according to manufacturer's instructions and photographed using a digital camera (Kodak DC40) equipped with SYPRO Orange photographic filter. The amount of undigested OPRTase remaining in each tryptic digest sample was quantitated using the Kodak Digital Science 1D software (Kodak).

Separation of Tryptic Digest by HPLC. Trypsin-digested WT (1.5 mg; about 60% inactivated) or K26A (1.5 mg; about 64% inactivated) OPRTase was applied onto a C4 column (Vydac 4.6 × 300 mm) and chromatographed at a flow rate of 2 mL/min in 0.1% TFA/H_2O using a 100 mL linear gradient to 100% acetonitrile. Peak fractions were collected and analyzed by mass spectrometry by Dr. Steven Seeholzer at the Fox Chase Institute for Cancer Research.

Construction and Purification of H105A OPRTase. To construct H105A OPRTase, we generated a silent mutation upstream of the loop coding sequence using the overlapping PCR method (*29*) to introduce a *Bgl*II site 5′ of the loop coding sequence. This *Bgl*II restriction site and a naturally occurring *Bss*HII site 3′ of the loop coding sequence enabled us to insert PCR fragments encoding any desired loop sequences. A 1 kb *Eco*RI−*Pst*I fragment from pCG13 (*30*) encoding the entire *pyrE* gene of *S. typhimurium* OPRTase was used as a template to introduce a *Bgl*II site (silent mutation) to the coding sequence (642 base pairs) using the overlapping PCR method (*29*). Oligonucleotide primers used were 5′ CACGATAAAGATCTGCCGTACTGC 3′ and 5′ GCAGTACGGCAGATCTTTATCGTG 3′. The 0.7 kb PCR product, containing the new *Bgl*II site, was digested with *Nde*I and *Bam*HI and ligated with T7 promoter vector pRSET C (Stratagene) previously digested with *Nde*I and *Bgl*II, yielding pGW01. The entire coding sequence was subjected to DNA sequencing using the Sequenase 2.0 kit (U. S. Biochemicals). To construct the H105A mutant, we employed overlapping PCR similarly using pGW01 as a template. The primers used were 5′ CAAAAGATGCTGGTGAAGGCGG 3′ and 5′ CTTCACCAGCATCTTTTGCCTCT 3′. To minimize subsequent DNA sequencing, we used *Bgl*II and *Bss*HII to digest the 0.7 kb PCR product carrying the mutation, and the 68 bp fragment was ligated with pGW01 previously cut with the same restriction endonucleases, resulting in a recombinant plasmid carrying the mutation in the coding sequence. The desired mutation was confirmed by DNA sequencing of the 68 bp loop region.

To overexpress WT and H105A OPRTase, we transformed the recombinant plasmid into T7 RNA polymerase *E. coli* host BL21(DE3) (*31*). Transformants were selected and purified on LB plates containing 50 μg/mL carbenicillin. Both WT and H105A constructs produced a high level of expression in the BL21(DE3) *E. coli* host. Enzymes were purified from 6 L cultures using the protocol described in Bhatia et al. (*30*) with modification (*32*), except that 0.1 mM PMSF was added to the cells prior to sonication. Approximately 200−250 mg of highly homogeneous OPRTase was typically isolated from 20 g of cells.

Standard Enzymatic Assays. Pyrophosphorolysis of OMP was monitored as an increase in absorbance at 302−304 nm as previously described (*32*). The standard forward reaction using orotate and PRPP as substrates was monitored as a decrease in absorbance over the same wavelength region. For each assay, the buffer mixture was allowed to reach thermal equilibrium in a 30 °C dry bath before addition of substrates followed by 0.05−0.1 μg of wild-type enzyme. For the less-active H105A OPRTase, the quantity of enzyme was increased as needed in order to produce measurable linear initial rates. One unit of activity was defined as the amount of enzyme needed to convert 1 μmol of orotate to OMP (or 1 μmol of OMP to orotate) per minute at 30 °C. For the calculation of k_{cat}, a subunit M_r value of 23 561 was used (*33*). The concentration of protein was determined spectrophotometrically at 280 nm as described in the previous paper.

Backbone ^{15}N Protein Labeling. To specifically label the backbone nitrogens of histidine or leucine residues in OPRTase, a 50 mL overnight culture of *E. coli* BL21(DE3) transformed with the wild-type plasmid pGW01 was inoculated into twelve flasks of 500 mL LeMaster medium (*34*) supplemented with [α-^{15}N]histidine or [α-^{15}N]leucine, Kao and Michayluk vitamin solution (*35*), and 50 μg/mL carbenicillin. Procedures for overexpression and purification of isotopically labeled enzymes were identical to those for the unlabeled wild-type and mutant enzymes.

NMR Sample Preparation. Enzymes for NMR spectroscopy were desalted by either G-50 gel filtration centrifugation (*36*) or Centricon 30 ultrafiltration. For ^1H-^{15}N heteronuclear NMR spectroscopy, the samples contained 2.2−2.7 mM ^{15}N-labeled OPRTase subunit in 80 mM Na-PIPES, 1 mM EDTA, 1 mM DTT, and 10% D_2O, pH 6.9. Under these conditions, OPRTase is stable at room temperature for at least 3 weeks. For proton NMR spectroscopy, enzyme was desalted and concentrated in 80 mM Na-PIPES and 1 mM EDTA in D_2O, pH* 7.2 (pH* indicates a pH meter reading uncorrected for deuterium isotope effect on a glass electrode), using a Centricon-30 concentrator. In the case of ^{31}P NMR, 80 mM Na−PIPES and 1 mM EDTA in H_2O, pH 6.9, was used.

PRPNP Synthesis. PRPNP was prepared enzymatically using *E. coli* PRPP synthase (a generous gift of Dr. R. Switzer). The synthesis reaction contained 20 mM AMPPNP (5′-adenylylimidodiphosphate), 40 mM ribose 5-phosphate, 30 mM $MgCl_2$, and 5 μg of PRPP synthase in 1.5 mL of 50 mM KH_2PO_4 and 50 mM triethanolamine at pH 8.0. The reaction mixture was incubated at 30 °C for 2 h before being applied to a 1 mL column of charcoal/Whatman CF11 cellulose (1:4, w:w; ref *37*) and eluted with 50 mM K_2HPO_4 at pH 8.0. The fractions containing PRPNP (assayed using human HGPRTase; ref *38*) were pooled and applied to a Mono-Q column (Pharmacia, 0.5 × 5 cm) previously equilibrated with 50 mM NH_4HCO_3 at pH 8.0. The column was eluted at a flow rate of 1 mL/min with a 20 mL linear gradient of 50−500 mM NH_4HCO_3 at pH 8.0. The fractions containing PRPNP were pooled, lyophilized, and resuspended in a desired buffer before storing at −20 °C.

Heteronuclear ^{15}N Spectroscopy and Relaxation Measurements. All ^{15}N NMR experiments were performed on a Bruker DRX-600 spectrometer at 27 °C. Gradient-enhanced two-dimensional ^1H-^{15}N HSQC experiments (*39*) were used

to observe backbone amide resonances in the three ^{15}N specifically labeled samples. Data were acquired with 2048 complex points in the direct dimension and 128 or 256 complex points in the indirect dimensions. Sweep widths were 7788 Hz in the proton dimension and 2500 Hz in the nitrogen dimension. Proton chemical shifts were referenced directly to internal TSP [3-(trimethylsilyl)-propionic acid]. Nitrogen referencing was calculated indirectly from the proton reference (*40*). All two-dimensional data were processed and analyzed using nmrPipe (*41*).

The pulse sequences used for measuring ^{15}N T_1 and T_2 relaxation times and $^{15}N\{^1H\}$ NOEs are described in Skelton et al. (*42*), and were modified to include watergate-based water suppression (*43*) as described in Fushman et al. (*44*). The NOE experiment was also modified to reduce magnetization exchange between the amide protons and water protons according to Grzesiek and Bax (*45*). Data sets for the T_1 and T_2 experiments were collected with 4096 and 192 complex points in F2 (^1H) and F1 (^{15}N) respectively, with 32 scans per t_1 point and a recycle delay of 1 s. Data sets for the NOE experiments were collected with 2048 and 64 complex points in F2 (^1H) and F1 (^{15}N), respectively, with 96 scans per t_1 point and a recycle delay of 6 s. All experiments used a proton sweep width of 7800 Hz and a ^{15}N sweep width of 2500 Hz with the ^1H and ^{15}N carriers set to 4.7 and 115 ppm, respectively.

The T_2 measurements were performed with the following transverse relaxation delays: 8, 16 (×2), 24, 32, 40, 48, 64 (×2), 128, 160, 240 (×2), and 320 ms, and a 1 ms delay was used between ^{15}N pulses in the Carr-Purcell-Meiboom-Gill sequence during the transverse relaxation period. The T_1 measurements were performed with the following longitudinal relaxation delays: 8, 20 (×2), 40, 100 (×2), 160, 200, 300 (×2), 500, and 800 ms, and 2 and 4 s. $^{15}N\{^1H\}$ steady-state NOE values were obtained by recording spectra with and without a 3 s GARP proton decoupling period (*46*) applied in the middle of the amide spectral region during the recycle delay.

Analysis of Relaxation Data. Spectra were processed with a 25 Hz exponential window function and zero-filled to yield data sets with 2048 and 256 points in F2 (^1H) and F1 (^{15}N), respectively. Peak intensities in the 2D spectra were measured using XEASY (*47*, *48*). The T_1 and T_2 values for each residue were determined by fitting the peak heights as a function of the relaxation delay, τ, using the program DFIT (*49*). The relaxation data were fit to a two parameter exponential decay:

$$I(\tau) = I_o \exp(-\tau/T_{1,2})$$

using Levenberg−Marquardt minimization, and parameter uncertainties were calculated by a Monte Carlo approach. The steady-state NOE values were determined from the ratios of cross-peak intensities in experiments recorded with and without ^1H saturation:

$$\text{NOE} = I_{sat}/I_{unsat}$$

Uncertainties in the calculated NOE values were determined by measuring the standard deviation of the baseplane noise in the spectra with and without ^1H saturation.

Backbone dynamics for each histidine residue were determined from the T_1, T_2, and $^{15}N\{^1H\}$ NOE values using the program DASHA 3.43 (*49*). The measured T_1, T_2, and $^{15}N\{^1H\}$ NOEs were interpreted using the model-free formalism introduced by Lipari and Szabo (*50*) and extended by Clore et al. (*51*). The theory of relaxation, the analysis of relaxation data, and the extraction of model-free parameters from relaxation parameters have been described in detail elsewhere (*44*, *52*, *53*). Briefly, for a given model of local motion, the parameters of internal motion for each residue, *i*, were obtained by minimization of the following penalty function:

$$\chi^2 = \Sigma_j \chi^2 = \Sigma_i \Sigma_k [R_k\text{clc}(q) - R_k \exp]^2/[\Delta R_k\text{exp}]^2$$

where the subscript *i* runs over all histidine residues, *q* is the set of adjustable parameters for the given model, subscript *k* is the set of calculated (clc) and measured (exp) experimental quantities (T_1, T_2, and NOE), and ΔR_kexp is the uncertainty in the measured experimental quantity. The selection of a model of local motion was based on a procedure similar to that employed by Mandel et al. (*52*) in which five models are considered: (1) S^2; (2) S^2, R_{ex}; (3) S^2, t_e; (4) S^2, t_e, R_{ex}; and (5) S_f^2, S_s^2, t_s where R_{ex} is the contribution to R_2 from chemical exchange occurring on the microsecond to millisecond time scale. Models 1-4 are based on the following form of the autocorrelation function:

$$C(t) = S^2 + (1 - S^2) \exp(-t/t_e)$$

where S^2 is the order parameter (equals 0 and 1 for completely unrestricted and completely restricted internal motion, respectively) for internal motion characterized by correlation time, t_e. Note that the above equation reduces to

$$C(t) = S^2$$

for very small values of t_e ($t_e \ll 20$ ps) which is assumed in models 1 and 2. Model 5, based on the following form of the autocorrelation function introduced by Clore et al. (*51*), assumes the presence of two uncorrelated sets of internal motions, a fast motion and slow motion:

$$C(t) = S_f^2 S_s^2 + (1 - S_f^2) \exp\left(-\frac{t}{t_f}\right) + (S_f^2 - S_f^2 S_s^2) \exp\left(-\frac{t}{t_s}\right)$$

where S_f^2 is the order parameter for fast internal motion characterized by correlation time, t_f, and S_s^2 is the order parameter for slow internal motion characterized by correlation time, t_s ($t_f \ll t_s < t_c$). For model 5, the program DASHA limits the number of adjustable parameters by assuming that t_f is very small thus making the second term in the above equation negligible. The appropriate model for each residue is selected by initially fitting the data to the simplest model (model 1) and resorting to more complex models only when required to fit the relaxation data. Furthermore, model selection for each residue was accompanied by a search for the optimal overall correlation time, t_c, which was assumed to be isotropic. A model for a given residue was considered appropriate when the χ_i value obtained for the model was smaller than the $\alpha = 0.05$ critical value of the χ_i distribution obtained from Monte Carlo simulations.

Proton NMR Spectroscopy. The 600 MHz NMR spectra were acquired on a Bruker 600 spectrometer. TSP (200 μM) [3-(trimethylsilyl)tetradeuteriosodium propionate] was added to each sample as an internal reference for proton chemical shift. For chemical exchange experiments, each wild-type enzyme sample (0.5−2 mM) containing 80 mM Na-PIPES, 1 mM EDTA, and 10 mM $MgCl_2$ in D_2O, pH* 7.2 was titrated with increasing amounts of PRPP (0−8 mM), OMP (0−2.4 mM), or PP_i (0−2 mM). In the case of Na_2SO_4 (0−100 mM) titration, experiments were performed in the absence of $MgCl_2$. A total of 64 transients were collected for each ligand concentration at 27 °C using a Hahn-echo pulse sequence (*54*), with 1.5 s delay between successive scans. In each experiment 16 384 data points were collected, using a 7788 Hz spectral width. Data were typically zero-filled to 32 768 points before Fourier transformation. In selected experiments, the signal-to-noise ratio was improved using an exponential function leading to a line broadening of 2−10 Hz. The C1H resonance of bound PRPP was identified by saturation transfer (*55*) from the well-resolved C1H of unbound PRPP.

^{31}P NMR Spectroscopy. ^{31}P spectra of free and enzyme-bound ligands were obtained on a Bruker DRX300 spectrometer at 22 °C. In titration experiments, each 0.5−2 mM WT enzyme sample containing 80 mM Na-PIPES, 1 mM EDTA, and 12 mM $MgCl_2$ in H_2O, pH 6.9 was titrated with 2−6 mM PRPP or 0.5−6 mM OMP. To obtain reasonable signal-to-noise ratios, 512 transients were necessary. The spectral width for each spectrum was 4200 Hz, and 8192 data points were acquired. Data were zero-filled to 32 768 points before Fourier transformation. A line-broadening function of 10 Hz was applied to all spectra prior to the measurement of linewidths.

Analysis of PRPP Titration Data. The linewidths of free PRPP C1H and 5-phosphate signals were monitored by ^{1}H and ^{31}P NMR, respectively, as a function of the ratio of bound to free ligand concentration, assuming a two-site exchange model (*56*). The off-rate of PRPP was determined from the slope of a plot of linewidths of free ligand signals versus the ratio of bound to free ligand concentration using a linear least-squares regression analysis.

For the protein resonance (His-105 C2H) in the titration, a full lineshape analysis was performed. The free and bound PRPP concentrations were determined on the basis of E_T, L_T, and the K_D values for PRPP (*27*). The resonance frequencies and $1/T_2$* values of the histidine C2H signals in the two states were measured at [PRPP] = 0 and 8 mM, respectively. Simulated spectra were calculated using lineshape analysis software (MEX, obtained from Dr. Alex Bain; refs *57*, *58*). The unidirectional rate constant between the two forms of the enzyme was determined by a visual best fit of the simulated spectra to the experimental data.

Analysis of Sulfate Titration Data. The C2H signal of His-105, assigned on the basis of H105A mutant enzyme spectra, was monitored as a function of sulfate concentration. The equilibrium binding constant (K_D) and ν_{bound} were determined by plotting the changes in C2 proton chemical shift versus total sulfate concentration and fitting the data by nonlinear least-squares regression to a hyperbolic equation using SigmaPlot (SPSS Inc.).

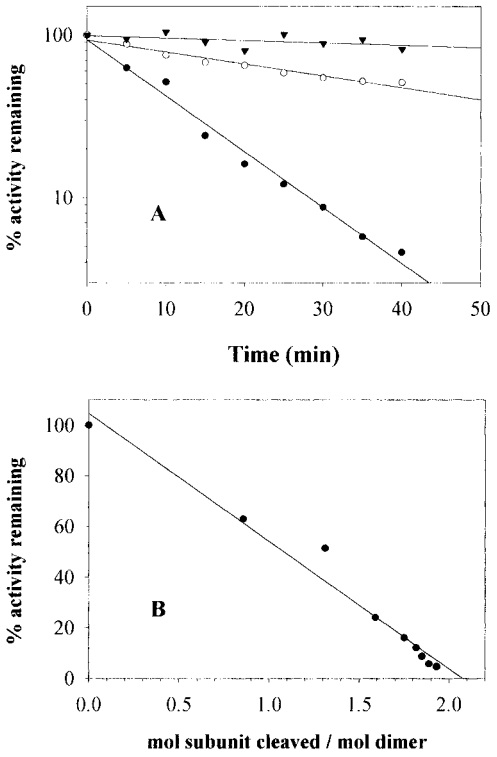

FIGURE 1: (A) Trypsin proteolysis of WT OPRTase. WT OPRTase (0.5 mg/mL) was subjected to trypsin (0.05 mg/mL) cleavage in the absence of protecting ligands (●), in the presence of 2 mM PRPP (○), or in the presence of 100 μM OMP (▼). The proteolysis reaction was quenched with 1 mM PMSF at the indicated times. The extent of enzymatic activity loss was monitored using the standard reverse pyrophosphorolysis assay. (B) A plot of the enzymatic activity loss versus the extent of trypsinolysis in WT OPRTase. PMSF-quenched trypsinolysis reactions were assayed for the remaining enzymatic activity and analyzed on a 15% SDS−PAGE for the quantitation of undigested enzyme. The data were fit using a linear least-squares regression analysis.

Table 1: Proteolysis of WT and K26A Mutant OPRTase

enzyme	protecting agent	$t_{1/2}$ (min)	k_{obs} (min^{-1})	fold protection
WT	none	8.8	7.9×10^{-2}	
	2 mM PRPP	41.3	1.7×10^{-2}	4.7
	100 μM OMP	203	3.4×10^{-3}	23.2
K26A	none	30.7	2.3×10^{-2}	
	2 mM PRPP	931	7.4×10^{-4}	30.4
	1 mM OMP	207	3.4×10^{-3}	6.7

RESULTS

Proteolysis of WT and K26A Mutant OPRTase. When WT OPRTase was treated with trypsin, the enzyme lost activity over time in a pseudo-first-order process ($k_{obs} = 0.079$ min^{-1}; Figure 1A). SDS−PAGE revealed the loss of protein from the $M_r = 24\,000$ band and the accumulation of metastable fragments at $M_r \approx 11\,000$ and 21 000 as inactivation proceeded. Substrate PRPP (2 mM) provided 4.7-fold protection against activity loss, whereas 100 μM OMP offered 23.2-fold protection (Figure 1A; Table 1). Digitization of images of SYPRO Orange stained gels showed that complete loss of enzymatic activity was correlated with the cleavage of 2 mol of subunit/mol of OPRTase dimer (Figure 1B). Cleavage products were isolated from partially inactivated enzyme by HPLC. Mass spectrometric analysis of cleavage products indicated that the primary inactivating tryptic cleavage site in WT was at Lys-26, located at the tip of the hood (an

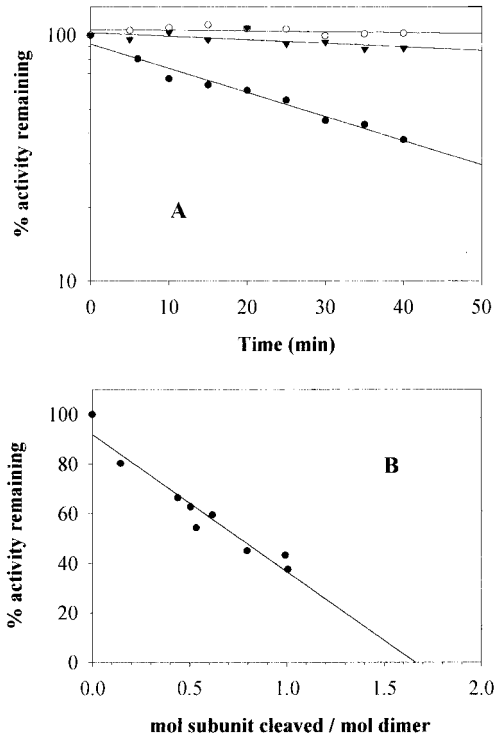

FIGURE 2: (A) Trypsin proteolysis of K26A OPRTase. K26A OPRTase (0.5 mg/mL) was subjected to trypsin (0.05 mg/mL) cleavage in the absence of protecting ligands (●), in the presence of 2 mM PRPP (○), or in the presence of 1 mM OMP (▼). Analysis of enzymatic activity loss over time was performed as described in Figure 1A. (B) A plot of the enzymatic activity loss versus the extent of trypsinolysis in K26A OPRTase, performed as in Figure 1B.

N-terminal β-hairpin structure partially covering the active site; ref *18*), resulting in accumulation of the 1−26 (M_r = 3205) and 27−213 (M_r = 20 375) peptide. Slower cleavages of the enzyme at Lys-103 and subsequently at Lys-100 were also observed.

To eliminate the cleavage site at Lys-26, we used the catalytically competent K26A OPRTase (*20*). When K26A was treated with trypsin, a slower pseudo-first-order loss of enzymatic activity was observed (k_{obs} = 0.023 min^{-1}; Figure 2A). With this mutant, 1 mM OMP gave 6.7-fold protection, whereas 2 mM PRPP provided at least 30-fold protection against trypsin digestion (Figure 2A, Table 1). The rate of activity loss in the presence of OMP was the same as that for OMP-protected WT. Analysis of the HPLC-resolved K26A tryptic digest by mass spectrometry showed a single major inactivating cleavage site at the loop region (Lys-103) followed by cleavage of the 1−103 fragment at Lys-100. Complete trypsin inactivation was correlated with cleavage of 1.7 mol of subunit/mol of OPRTase dimer (Figure 2B). Proteolysis results confirmed the solvent-exposed position of Lys-103 in unliganded OPRTase, and indicate that binding of PRPP is associated with loop movement to a less exposed position.

Two-Dimensional ^{1}H-^{15}N Heteronuclear NMR Spectroscopy and ^{15}N Relaxation. Segmental motions in proteins can be assessed by studying the relaxation properties of backbone amide nitrogens (*53*). Due to the large size of the OPRTase dimer (47.1 kDa), specific ^{15}N labeling was chosen over uniform labeling for the loop dynamics studies. His-105, positioned at the tip of the surface loop, provided a

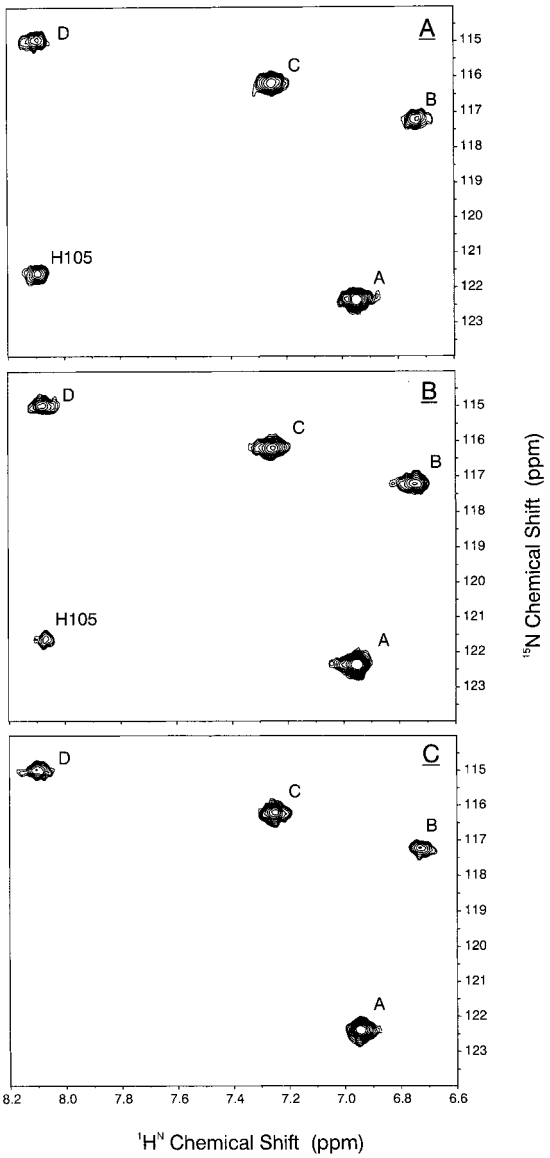

FIGURE 3: ^{1}H-^{15}N HSQC spectra of backbone [^{15}N-His]OPRTase. All spectra are of ~2.5 mM enzyme subunit, at 27 °C. (A) Spectrum for the unliganded WT protein. (B) Spectrum after the addition of 7.5 mM PRPNP. Note the reduction in intensity of the cross-peak labeled as H105. (C) Spectrum of the H105A protein. The cross-peak labeled as H105 in panels (A) and (B) is missing. All other His cross-peaks are unaffected relative to the WT spectrum in panel (A).

convenient probe for studying the motional properties of the flexible loop. *Salmonella* OPRTase contains only five histidine residues (at positions 88, 89, 105, 143, and 200). The α-nitrogens of histidines were labeled with ^{15}N by growing cells in a rich defined medium supplemented with [α-^{15}N]histidine. The 2D ^{1}H-^{15}N HSQC spectrum of [α-^{15}N]-histidine-labeled WT OPRTase is shown in Figure 3A. All five expected cross-peaks were observed and resolved. The His-105 cross-peak was unambiguously identified on the basis of the [α-^{15}N]histidine-labeled H105A mutant OPRTase spectrum (Figure 3C). The other four peaks were designated A−D. Titration of [α-^{15}N]histidine-labeled WT OPRTase with PRPNP, a stable PRPP analogue, showed that the resonance of His-105 first broadened, then became nearly undetectable, and finally reappeared as the PRPNP concentration was increased to saturate the enzyme. No changes in

Table 2: Relaxation Parameters for Histidine Backbone Nitrogen Atoms of Unliganded [α-^{15}N]Histidine-Labeled WT OPRTase

His	T_1 (s)	SD[a]	T_2 (ms)	SD	NOE	SD	S^2	SD	S_s^2	SD	S_f^2	SD	τ_e/τ_s (ns)	SD
A	2.211	0.096	22.0	0.6	0.65	0.05	0.946	0.019	0.964	0.006	0.982	0.014	0.792	0.142
105	0.822	0.045	56.9	1.8	0.32	0.06	0.337	0.014	0.424	0.009	0.796	0.015	1.335	0.042
B	2.627	0.231	25.7	1.8	0.56	0.09	0.833	0.021					0.026	0.005
C	2.470	0.323	21.9	0.6	0.77	0.08	0.954	0.016						
D	2.545	0.168	20.7	1.1	0.79	0.07	0.988	0.018						

[a] Standard deviation.

either the ^{1}H or ^{15}N chemical shifts were observed throughout the titration. The other histidine amide resonances (A−D) were unaffected by PRPNP. The low signal intensity of the His-105 cross-peak at the highest PRPNP concentration utilized (Figure 3B) prohibited relaxation studies of the ligand-saturated enzyme by the two-dimensional technique.

^{15}N relaxation measurements were performed to characterize the motion of the loop backbone. The T_1, T_2, and ^{15}N-{^{1}H} NOE values are given in Table 2. It is clear that the His-105 T_1, T_2, and ^{15}N{^{1}H} NOE values differ significantly from those of the other histidine residues. The model-free parameters for each histidine residue obtained by fitting the relaxation data are given in Table 2. An isotropic model of motion was used in the fitting procedure, and the overall isotropic correlation time that best fit the data was 34.8 ns.

The relaxation data of two residues, C and D, could be fit satisfactorily using a model in which the system is characterized by only a single parameter for the internal motion, S^2, and the correlation time for internal motion is assumed to be very small (≪10 ps). The relaxation data of a third residue, B, could be fit using a model in which the system is characterized by an order parameter, S^2, and a correlation time for internal motion, t_e. The high order parameters ($S^2 > 0.94$) and very low t_e values suggest that these three residues belong to structured regions of the enzyme. Consistent with these observations, three histidine residues (His-88, His-89, and His-200) are located in the A3 and A7 helices of the enzyme, and have relatively low temperature factors (25−33 Å^2) in the crystal structure (*18, 19*).

The relaxation data for the two remaining residues, A and His-105, could only be satisfactorily fit using an extended form of the autocorrelation function, characterized by the parameters S_s^2, S_f^2, and t_s. If residues B, C, and D are assigned to residues that are found in structured regions of the protein (His-88, His-89, and His-200) as discussed above, residue A is His-143. His-143 is located in a small loop joining α-helix A4 and β-strand B4 in the enzyme. The temperature factor for the amide nitrogen of His-143 in the two crystal structures was higher (56.1 and 47.1 Å^2) than those for His-88, His-89, and His-200 amide nitrogens (*18, 19*), and would likely show greater flexiblity than those residues in the structured regions of the enzyme.

His-105 is located in the surface-exposed catalytic loop of the enzyme between β-strands B2 and B3. This residue belongs to a cluster of residues (103−107) that show very weak electron density and could not be satisfactorily fit in various crystal structures of the protein (*18, 19*). The extremely low order parameter of 0.34 for His-105 based on relaxation measurements in solution is consistent with its disorder in the crystal structures. It should be noted that an R_{ex} term was not needed to satisfactorily model the relaxation behavior of any of the histidine residues in the enzyme, suggesting that either a low-frequency exchange process in the microsecond to millisecond time scale is not significant for these residues or the ^{15}N T_2 relaxation experiment is not sensitive to the exchange process (i.e., the chemical shift difference for the exchange process is small).

Chemical Exchange NMR Spectroscopy

PRPP Titration. Proton NMR spectra of WT OPRTase in the aromatic region (Figure 4) showed five well-resolved histidine C2H resonances. The most downfield peak was definitively assigned to His-105 C2H on the basis of its absence in the H105A OPRTase spectrum. Upon titration with PRPP, the His-105 C2H resonance of WT broadened and shifted progressively downfield as PRPP concentration became equimolar with the concentration of OPRTase dimer. At higher PRPP concentration, the peak intensity increased. The His-105 C2H resonance was clearly in the intermediate exchange regime, permitting the determination of rate constants for PRPP binding. The results of lineshape simulations are shown in Figure 4 as dotted lines. The unidirectional rate constant (from bound to free enzyme resonance) that provided the best visual fit to the experimental spectra was 400 s^{-1}. Values below 300 s^{-1} or above 500 s^{-1} did not provide a good fit to the data. The value of 400 s^{-1} represents the rate at which His-105 in its "loop-closed" conformer can produce its "loop-open" conformer, when the active site is occupied by PRPP. Two other resonances (7.95 and 7.70 ppm) also showed signs of peak broadening and/or shifting during titration. Simulations were not performed on these resonances due to their minimal changes and signal overlaps.

The C1H resonance of unbound PRPP (5.8 ppm) was well-resolved in a region free of protein signals (Figure 5A). The bound C1H resonance was identified at 6.2 ppm using the saturation transfer technique. Thus the C1H of unbound PRPP was clearly in slow exchange with the bound C1H signal, allowing us to measure the rate of exchange between bound and free PRPP using linewidth analysis (*59*). The analysis employed a two-site exchange model, in which the ligand PRPP can equilibrate between bound (6.2 ppm) and free (5.8 ppm) forms (*56*). A plot of $1/T_2$* for the C1H of unbound PRPP (calculated from the measured linewidths) versus the ratio of bound to free PRPP gave a straight line whose slope represents the off-rate (69 ± 2 s^{-1}) of PRPP (Figure 5B).

The 5-phosphate resonances of free and bound PRPP were also in slow exchange (spectra not shown). A linear least-squares plot of $1/T_2$* versus the ratio of bound to free PRPP gave an off-rate of 73 ± 5 s^{-1} for PRPP (Figure 6), which was comparable to that obtained with PRPP C1H linewidth analysis (69 s^{-1}) but significantly slower than the rate (400 s^{-1}) determined from His-105 C2H lineshape analysis.

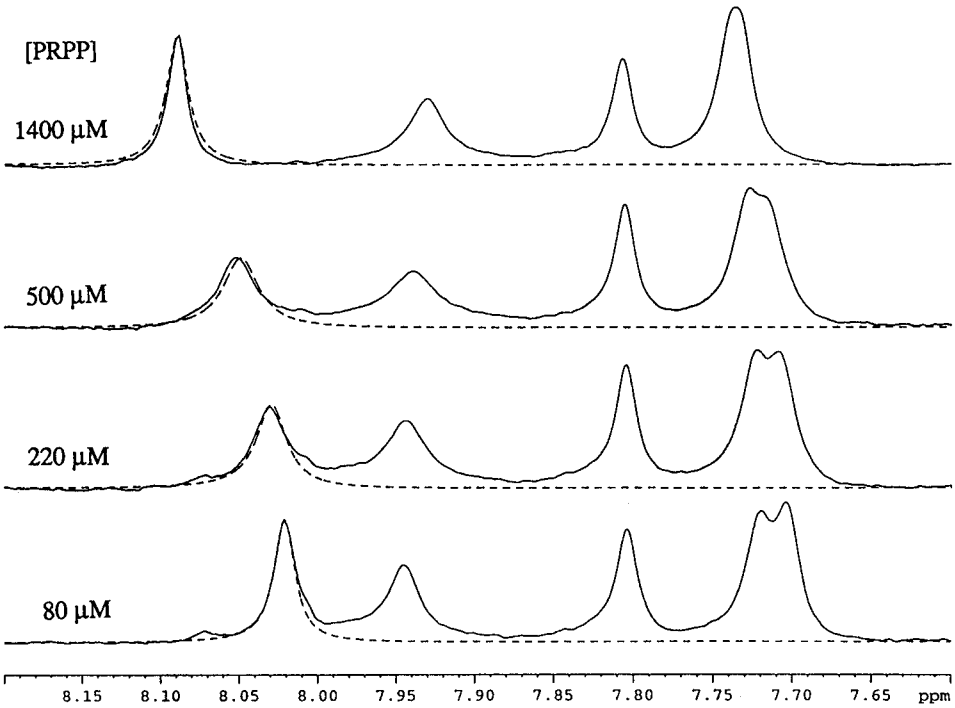

FIGURE 4: Titration of histidine C2 proton resonances of 2 mM WT OPRTase by PRPP. Five distinct peaks are clearly observed, each corresponding to a histidine C2 proton. The proton resonance at 8.02 ppm in the presence of 80 μM PRPP is the His-105 C2 proton, identified on the basis of its absence in the H105A mutant enzyme spectrum. Lineshape simulations (see text) for the His-105 C2 proton resonances using a rate of 400 s^{-1} are shown as dotted lines.

Sulfate Titration. Sulfate is a weak inhibitor of OPRTase and binds in the position of the β-phosphate of PRPP (ref *23*; K_I for sulfate in *E. coli* OPRTase is estimated to be approximately 3 mM). The ^{1}H protein spectra of sulfate titration (Figure 7A) showed that the His-105 resonance was in a fast exchange regime. A plot of C2 proton chemical shift versus total sulfate concentration (Figure 7B) gave a K_D of 15.2 $\pm$ 0.5 mM for sulfate. The off-rate for sulfate could not be determined from the NMR data, although a lower limit (2400 s^{-1}) could be estimated on the basis of chemical shifts and lineshape analysis (*59*).

PP_i Titration. With increasing concentrations of MgPPi, the His-105 C2H resonance shifted progressively downfield and broadened, giving a titration pattern much like that observed in PRPP titration (spectra not shown). Precipitation of MgPPi above 2 mM, however, precluded lineshape analysis to obtain rate data.

DISCUSSION

This work is the first attempt to quantitate the rate of loop movement in Type I nucleotide synthases, and to relate loop dynamics to enzymatic catalysis. We have employed proteolysis and NMR techniques to show that loop movement occurs in solution and is influenced by ligands. We first discuss dynamics of the flexible loop structure, then proteolysis to assign loop conformational states, and finally a proposed model that describes the rates of loop motion in catalysis.

Backbone Dynamics of the Flexible Loop. All known Type I PRTase structures contain surface loops atop solvent-exposed active sites. It has been proposed that the surface loop descends and occludes the active site during the phosphoribosyl group transfer reaction. In OPRTase, the loop residues are highly conserved. Several loop residues are important for catalysis (*20*), although their catalytic roles have not been characterized in detail. In HGPRTase, the highly conserved Ser-Tyr dyad on the loop has been shown to be catalytically important (*26*). Other PRTase structures showing flexible loops in down conformations covering the catalytic pocket (*23*−*25*) further highlight the importance of loop closure in PRTases.

The ^{15}N relaxation results clearly demonstrate that the backbone of the loop at His-105 is highly flexible in solution. The relaxation data for His-105 were accurately reproduced only when an extended parameter set was used during the modeling procedure, indicating the existence of internal motions of significant amplitude both on the very fast (extreme narrowing) and relatively slow time scales (*51*). Such behavior is often observed for residues in unstructured regions (e.g., N- and C-termini), for residues in very flexible loops, and for residues serving as hinges for loop movements. The data presented here for a single residue in the OPRTase loop cannot distinguish among these possibilities. If the motion corresponded to a simple rigid-body opening and closing of the loop, one could interpret the order parameter for slow motion within the framework of a two-site model to develop a more physical picture of the scale of the motion (*51*):

$$S_s^2 = (1 + 3\cos^2\phi)/4$$

where ϕ is the angle between the two orientations of the N−H bond. The H105 S_s^2 value of 0.4 and τ_e value of 1.3 ns correspond to fluctuations of ~60° on the nanosecond time scale.

The structure of the loop in its open and closed forms, as well as the dynamics of its exchange between these two states in the presence and absence of ligand, are of great interest.

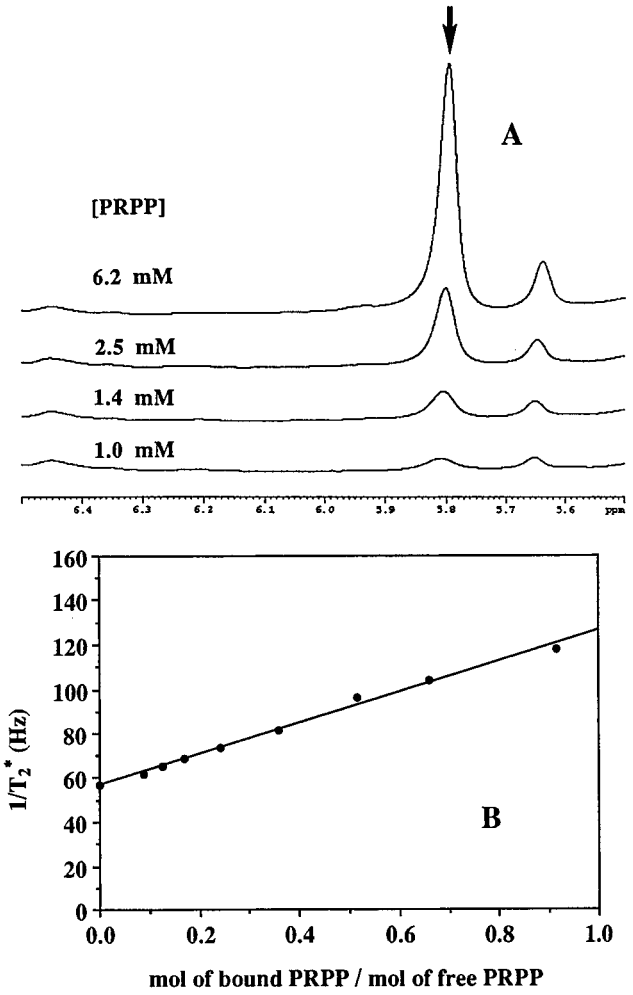

FIGURE 5: ^{1}H NMR PRPP titration of 0.5 mM OPRTase. (A) C1 proton resonance of unbound PRPP is at 5.8 ppm (arrow). The C1H signal of enzyme-bound PRPP (6.2 ppm) was identified using saturation transfer as described in Experimental Procedures. (B) A linear least-squares plot of $1/T_2$* versus bound/free PRPP in the titration of WT OPRTase by PRPP. The values of $1/T_2$* were determined by measuring the linewidths of free PRPP C1 proton resonance. The ratios of bound/free PRPP were calculated on the basis of the known dissociation constant for PRPP (*27*). The slope of the line (69 s^{-1}) represents the dissociation rate constant of PRPP.

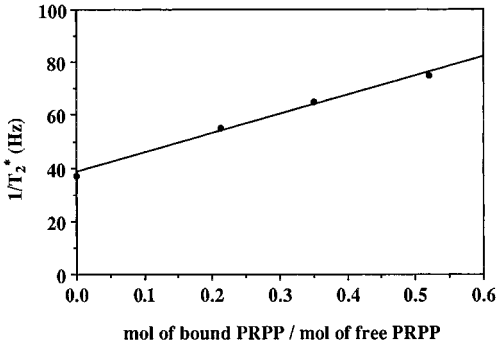

FIGURE 6: ^{31}P NMR PRPP titration of 0.5 mM OPRTase. The values of $1/T_2$* were determined by measuring the linewidths of free PRPP 5-phosphate resonance. The ratios of bound/free PRPP were calculated according to the known value of K_D. The slope of the linear least-squares line (73 s^{-1}) represents the dissociation rate constant of PRPP.

The effects of added PRPNP on the His-105 cross-peak in the HSQC spectrum indicate that the dynamic properties of the loop backbone change significantly upon ligand binding.

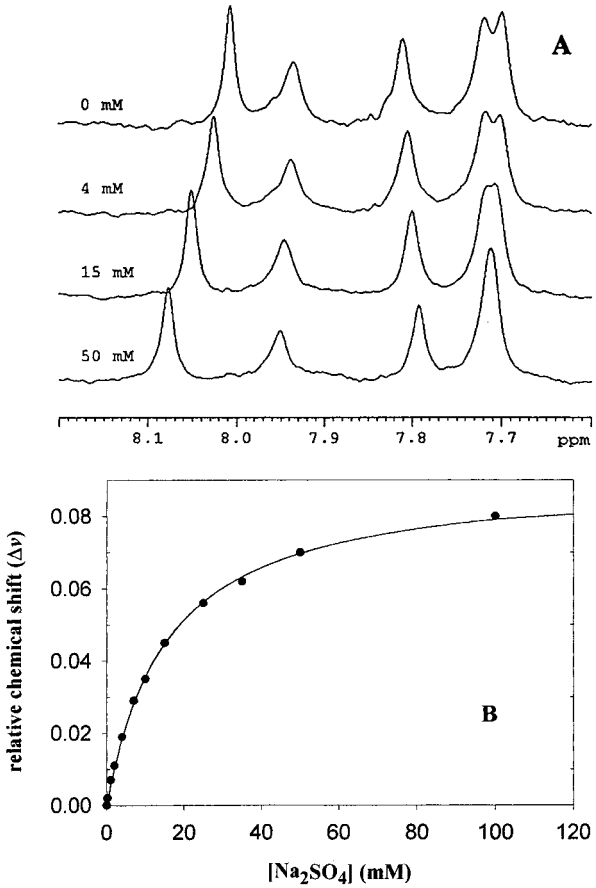

FIGURE 7: (A) Titration of histidine C2 proton resonances of 540 μM WT OPRTase by Na_2SO_4, showing fast exchange. The His-105 C2 proton at 8.02 ppm shifts progressively downfield as the Na_2SO_4 concentration increases (0−50 mM). A lower limit for the off-rate of sulfate (2400 s^{-1}) was estimated on the basis of chemical shift changes. (B) A plot of His-105 C2 proton chemical shift changes versus total sulfate concentration. The curve represents a best fit by nonlinear least-squares regression using the equation $\Delta\nu = \nu_{max}(L_f/K_D + L_f)$, where ν_{max} is the maximal chemical shift change at saturating Na_2SO_4 concentration, and L_f, or free Na_2SO_4 concentration, is given by $L_T - 0.5((K_D + E_T + L_T) - ((K_D + E_T + L_T)^2 - 4E_TL_T)^{1/2})$. E_T and L_T are total enzyme and Na_2SO_4 concentrations, respectively. The K_D value derived from the best fit curve was 15.2 mM.

Characterization of the dynamics in the presence of ligand was not possible due to the low intensity of the His-105 cross-peak in the PRPNP-saturated form of the enzyme. Future work is directed at examining the properties of other residues in the loop and at developing conditions for studying the ligated enzyme.

Proteolysis Studies. In the preceding paper (*27*), we show that the phosphoribosyl transfer chemistry in OPRTase is rapid, reaching on-enzyme equilibrium, with slow product release. The rate dependence of OPRTase reactions on solvent viscosity indicates that the slow product release is associated with a physical process (e.g., loop movement) which significantly limits the rate of net forward catalysis and is partially rate-limiting in the reverse reaction.

Susceptibility of both the hood region and the flexible loop to trypsin cleavage in WT enzyme prompted us to use a catalytically competent mutant, K26A, to simplify the study of loop conformations and to obviate any contribution from cleavage of the hood. Assuming that the major inactivating cleavage of K26A by trypsin is at Lys-103, the rate of

Scheme 1

$$K_{loop} = \frac{k_{open}}{k_{close}}$$

$$E_{closed}\cdot PRPP \underset{k_{close}}{\overset{k_{open}}{\rightleftharpoons}} E_{open}\cdot PRPP \underset{k_{assoc(PRPP)}}{\overset{k_{diss(PRPP)}}{\rightleftharpoons}} E_{open} + PRPP$$

cleavage at this location on the flexible loop was 2.3×10^{-2} min^{-1} (Table 1). The ligand PRPP (2 mM) slowed the rate of inactivation of K26A by about 30-fold (7.4×10^{-4} min^{-1}). The sluggishness of the inactivation hindered demonstration that the observed inactivation of PRPP-protected enzyme was still due to cleavage at Lys-103. Nevertheless, it was apparent from SDS−PAGE that this cleavage site was highly sequestered by the active site occupancy of PRPP. We have associated these trypsin-accessible and trypsin-inaccessible conformers of the E·PRPP binary complex with the loop-open (E_{open}·PRPP) and loop-closed (E_{closed}·PRPP) forms of the enzyme, respectively (Scheme 1). By assuming that the rates of inactivation (k_{inact}) by trypsin are the same for E_{open} and E_{open}·PRPP, we determined that the flexible loop in the E·PRPP complex favors the closed position by at least 30-fold ($K_{loop} = k_{open}/k_{close} = 0.033$). A finite value for K_{loop} was anticipated on the basis of the observation that PRPP provided substantial, but not absolute, protection of lysine residues on the loop from the small molecule modifier trinitrobenzene sulfonate (*32*). This equilibrium relationship is utilized below in the construction of a model to describe the kinetics of loop movement.

OMP protects K26A from tryptic digestion (6.7-fold; the rate of inactivation was 3.4×10^{-3} min^{-1} in K26A) to a lesser extent than does PRPP. Interestingly, this rate of inactivation was identical to that observed for OMP-protected WT (3.4×10^{-3} min^{-1}). Since in the presence of OMP the only detectable cleavage products on SDS−PAGE from both enzymes resulted from cleavage at the flexible loop, these inactivation rates are likely to represent the rate of loop cleavage in OMP-protected enzyme. Following the same logic as described above for PRPP protection from trypsinolysis, we determined the loop equilibrium (E_{closed}·OMP/E_{open}·OMP) in the E·OMP binary complex to be approximately 6.

In WT enzyme, the hood region is sensitive to tryptic cleavage at Lys-26. Residues in the hood are known to interact with orotate and the orotate moiety of OMP (*18*, *19*). Thus in OMP-protected WT, as expected, no cleavage at the hood was observed on SDS−PAGE under the proteolytic conditions utilized in this study. If the rate of cleavage at Lys-26 is represented by the observed rate of inactivation in unprotected WT (7.9×10^{-2} min^{-1}), its cleavage rate when protected by OMP must be reduced to less than 3.4×10^{-3} min^{-1}, the rate at which the flexible loop is digested, for proteolytic cleavage at the hood to be undetectable on SDS−PAGE. Thus it can be extrapolated that OMP protects the hood region from trypsinolysis by at least 23-fold, which may be attributed to the apparent formation of a hydrogen bond between the ϵ-amino group of Lys-26 and the 2′ and 3′ hydroxyl groups of the bound OMP (*18*).

PRPP provides only limited protection of the hood in WT, less than 4.7-fold. The rate of cleavage of the hood was at most 7.9×10^{-2} min^{-1}, the observed rate of inactivation in unprotected WT. PRPP (2 mM) slowed the inactivation rate to 1.7×10^{-2} min^{-1}. This rate represents the rate of cleavage at the hood, a conclusion well-supported by SDS−PAGE analysis and by the excellent ability of PRPP to prevent loop cleavage (7.4×10^{-4} min^{-1}). It is not clear why PRPP binding may produce changes in the conformational states of the hood. We speculate that this PRPP-induced conformational change of the orotate-binding hood region may partially account for the discrepancy between the values of K_D (280 μM) and K_M (20 μM) for orotate.

NMR Titrations. Lys-103, an essential loop residue (*20*), participates in catalysis at the adjacent active site (*21*), but is distant from the active site in the two known crystal structures. In this report, another flexible loop residue, His-105, is shown to exchange between two distinct environments in response to PRPP binding. We attribute these two environments to the loop-open (E_{open}) and loop-closed (E_{closed}) conformers of the enzyme (Scheme 1). In the loop-open form (E_{open} or E_{open}·PRPP; irrespective of its ligation state), His-105 on the flexible peptide loop is solvent-exposed, whereas in the loop-closed form (E_{closed}·PRPP), the residue is likely to be positioned in the vicinity of the PRPP-bound active site. The exchange rate (400 s^{-1}) obtained from our lineshape analysis of the C2H of His-105 thus represents k_{open}, the rate of loop opening for the E·PRPP complex. Existence of the loop-closed E·PRPP binary complex (E_{close}·PRPP) has been supported by the observation that PRPP protects a trypsin-sensitive cleavage site (Lys-103) on the flexible loop from proteolytic digestion, and by several reports of closed, loop-down PRTase structures. In *E. coli* GPATase complexed with substrate analogues of glutamine and PRPP, the flexible PRTase loop is seen atop the active site completely occluding the PRTase catalytic pocket in an active enzyme complex (*25*).

The ligand PRPP also exchanges between two distinct environments. To obtain exchange rates, we monitored the C1 proton and 5-phosphate of PRPP in independent titration experiments. The unidirectional rate constants for C1 proton and 5-phosphate from the bound (E_{closed}·PRPP or E_{open}·PRPP; irrespective of the positions of the flexible loop) to free PRPP were 69 and 73 s^{-1}, respectively, averaging to 71 s^{-1}. This averaged PRPP off-rate (k_{off}) represents the effective off-rate for enzyme-bound PRPP from both binary complexes (E_{closed}·PRPP + E_{open}·PRPP) and is used below in the determination of rates of loop movement.

The observation that PP_i and sulfate also significantly shift the His-105 C2 proton resonance indicates that loop closure also occurs upon binding of these ligands. In support of these titration results, the loop-down conformation with bound sulfate has already been seen in the highly homologous (97% identity) *E. coli* OPRTase. Due to the fast-exchanged C2 proton resonance in the sulfate titration, only the lower limit of the exchange rate constant (2400 s^{-1}) could be estimated. This rate constant represents the minimal rate for loop opening in the E·SO_4 binary complex (compared to 400 s^{-1} in the E·PRPP complex). Thus the rate of loop opening is ligand-dependent. Binding of PP_i is also likely to be associated with loop closure. In the *S. typhimurium* structure complexed with PRPP and orotate, the PP_i moiety of PRPP lies adjacent to the flexible loop. Unfortunately, precipitation of MgPPi and its weak binding to unliganded OPRTase have

Table 3: Rate Constants for a Two-Step Model of PRPP Release

rate constant	value	comment
k_{open}	400 s^{-1}	His-105 C2H titration with PRPP
k_{close}	12 000 s^{-1}	k_{open}/K_{loop}
$k_{diss(PRPP)}$	2200 s^{-1}	$k_{off} \times (k_{open} + k_{close})/k_{open}$
$k_{assoc(PRPP)}$	2.2×10^6 M^{-1} s^{-1}	$k_{off}/K_{D(PRPP)}$

thus far hindered detailed quantitative rate analysis.

Protection of the flexible loop from tryptic digestion by OMP suggests loop closure upon OMP binding. However, the His-105 C2 proton resonance was not significantly perturbed by OMP binding, preventing us from obtaining rate data.

Kinetics of Flexible Loop Movement. On the basis of the PRPP binding data (*27*), proteolysis results, and ^1H and ^{31}P NMR chemical exchange studies, movement of the flexible loop in OPRTase in response to PRPP binding is best described by a two-step model (Scheme 1) in which PRPP dissociation from the enzyme follows the opening of the flexible loop. An assumption of the model is that the enzyme exists in only two conformers: the loop-open form (E_{open}) and the loop-closed form (E_{closed}). The rate constants for Scheme 1 are tabulated (Table 3). We first discuss the derivation of these rate constants and then the general features of the proposed model.

The rate constant (400 s^{-1}) obtained from lineshape analysis of the His-105 C2 proton resonance is equal to k_{open}. The value of 0.033 for K_{loop} (k_{open}/k_{close}) obtained from proteolysis studies was used to calculate k_{close} (12 000 s^{-1}). Lower values for K_{loop} (in which the loop equilibrium favors the closed position by *more than* 30-fold) could also be accommodated by our data. The measured off-rate for PRPP (k_{off} = 71 s^{-1}), obtained from two independent NMR chemical exchange experiments, represents the effective off-rate of PRPP from all PRPP-containing complexes (i.e., E_{closed}·PRPP + E_{open}·PRPP), and is given by $k_{diss(PRPP)}$ multiplied by the fraction ($k_{open}/(k_{open} + k_{close})$) of the binary complexes that are in the form of E_{open}·PRPP. The value of $k_{diss(PRPP)}$ of 2200 s^{-1} was thus determined from the equation

$$k_{diss(PRPP)} = k_{off}(k_{open} + k_{close})/k_{open}$$

The known equilibrium binding constant (K_D) for PRPP (33 μM; ref *27*) then allowed calculation of $k_{assoc(PRPP)}$ (2.2×10^6 M^{-1} s^{-1}) on the basis of the equation

$$k_{assoc(PRPP)} = k_{off}/K_{D(PRPP)}$$

The values of k_{off} and $k_{assoc(PRPP)}$ represent k_{-1} and k_1, respectively, in the PRPP binding equilibrium in Scheme 1 of the accompanying paper (*27*). The k_1 value (2.2×10^6 M^{-1} s^{-1}) calculated here is in good agreement with the $k_{cat}/K_{M(PRPP)}$ value of 6×10^6 M^{-1} s^{-1} determined at 30 °C. A lower value for K_{loop} would yield proportionally higher rates for k_{close} and $k_{diss(PRPP)}$.

An essential feature of Scheme 1 is a moderately fast loop opening event (k_{open} = 400 s^{-1}) associated with an unfavorable partition between PRPP dissociation from the open active site ($k_{diss(PRPP)}$ = 2200 s^{-1}) and rapid loop closure (k_{close} = 12 000 s^{-1}). As a result, when the flexible loop opens to a transient solvent-extended position in the binary complex E_{open}·PRPP, only approximately 15% of the time does PRPP diffuse out of the open active site before rapid loop closure occurs. The rate of loop opening for other liganded E_{closed} complexes (E_{closed}·SO_4 or E_{closed}·PP_i) may be much faster (for E_{closed}·SO_4; $\geq$2400 s^{-1}).

The current model considers that the flexible loop in the unliganded enzyme stays in the open state. We were unable to document the existence of a loop-closed apoenzyme using the experimental techniques utilized in this study. However, the sensitivity of Lys-103 toward proteolysis and the behavior of His-105 C2H in PRPP titration indicate that the loop is predominantly open in the apoenzyme. Although it remains uncertain whether loop closure in OPRTase is ligand-gated or is an equilibrium event, our proposed scheme can accommodate either. In the equilibrium model, the flexible loop in the unliganded enzyme would remain mostly open but could fluctuate between the open and closed states. In either case, descent of the loop, an energetically unfavorable event, is driven by enzyme·PRPP interactions. The full binding energy of PRPP is thus not completely realized in its K_D but is in part used to stabilize the enzyme form associated with the transition state, the type of transforming event anticipated by Jencks as the "Circe effect" (*60*).

ACKNOWLEDGMENT

Gary Wang was supported through the M.D./Ph.D. program of Temple University School of Medicine. We are grateful to Dr. Steven Seeholzer at Institute for Cancer Research for performing mass spectrometric analysis. We also thank Dr. Peter Walsh for the use of the digital camera, and Dr. Alex Bain for providing the lineshape analysis software.

REFERENCES

1. Knowles, J. R. (1991) *Philos. Trans. R. Soc. London, Ser. B 322*, 115.
2. Falzone, C. J., Wright, P. E., and Benkovic, S. J. (1994) *Biochemistry 33*, 439−442.
3. Farnum, M. F., Magde, D., Howell, E. E., Hirai, J. T., Warren, M. S., Grimsley, J. K., and Kraut, J. (1991) *Biochemistry 30*, 11567−11579.
4. Li, L., Falzone, C. J., Wright, P. E., and Benkovic, S. J. (1992) *Biochemistry 31*, 7826−7833.
5. Williams, J. C., and McDermott, A. E. (1995) *Biochemistry 34*, 8309−8319.
6. Pompliano, D. L., Peyman, A., and Knowles, J. R. (1990) *Biochemistry 29*, 3186−3194.
7. Koshland, D. E., Jr. (1958) *Proc. Natl. Acad. Sci. U.S.A. 44*, 98−104.
8. Juszczak, L. J., Zhang, Z.-Y., Wu, L., Gottfried, D. S., and Eads, D. D. (1997) *Biochemistry 36*, 2227−2236.
9. Gerstein, M., Lesk, A. M., and Chothia, C. (1994) *Biochemistry 33*, 6739−6749.
10. Qian, M., Spinelli, S., Driguez, H., and Payan, F. (1997) *Protein Sci. 6*, 2285−2296.
11. Landry, S. J., Zeilstra-Ryalls, J., Fayet, O., Georgopoulos, C., and Gierasch, L. M. (1993) *Nature 364*, 255−258.
12. Landry, S. J., Taher, A., Georgopoulos, C., and van der Vies, S. M. (1996) *Proc. Natl. Acad. Sci. U.S.A. 93*, 11622−11627.
13. Markus, M. A., Hinck, A. P., Huang, S., Draper, D. E., and Torchia, D. A. (1997) *Nat. Struct. Biol. 4*, 70−77.
14. Derreumaux, P., and Schlick, T. (1998) *Biophys. J. 74*, 72−81.
15. Lolis, E., and Petsko, G. A. (1990) *Biochemistry 29*, 6619−6625.
16. Joseph, D., Petsko, G. A., and Karplus, M. (1990) *Science 249*, 1425−1428.

17. Tao, W., Grubmeyer, C., and Blanchard, J. S. (1996) *Biochemistry 35*, 14−21.
18. Scapin, G., Grubmeyer, C., and Sacchettini, J. C. (1994) *Biochemistry 33*, 1287−1294.
19. Scapin, G., Ozturk, D. H., Grubmeyer, C., and Sacchettini, J. C. (1995) *Biochemistry 34*, 10744−10754.
20. Ozturk, D. H., Dorfman, R. H., Scapin, G., Sacchettini, J. C., and Grubmeyer, C. (1995) *Biochemistry 34*, 10755−10763.
21. Ozturk, D. H., Dorfman, R. H., Scapin, G., Sacchettini, J. C., and Grubmeyer, C. (1995) *Biochemistry 34*, 10764−10770.
22. Eads, J. C., Ozturk, D., Grubmeyer, C., and Sacchettini, J. C. (1997) *Structure 5*, 47−58.
23. Henriksen, A., Aghajari, N., Jensen, K. F., and Gajhede, M. (1996) *Biochemistry 35*, 3803−3809.
24. Schumacher, M. A., Carter, D., Roos, D. S., Ullman, B., and Brennan, R. G. (1996) *Nat. Struct. Biol. 3*, 881−887.
25. Krahn, J. M., Kim, J. H., Burns, M. R., Parry, R. J., Zalkin, H., and Smith, J. L. (1997) *Biochemistry 36*, 11061−11068.
26. Jardim, A., and Ullman, B. (1997) *J. Biol. Chem. 272*, 8967−8973.
27. Wang, G. P., Lundegaard, C., Jensen, K. F., and Grubmeyer, C. (1999) *Biochemistry 38*, 275−283.
28. Laemmli, U. K. (1970) *Nature 16*, 680−685.
29. Ho, J. N., Hunt, H. D., Horton, R. M., Pullen, J. K., and Pease, L. R. (1989) *Gene 77*, 51−59.
30. Bhatia, M. B., Vinitsky, A., and Grubmeyer, C. (1990) *Biochemistry 29*, 10480−10487.
31. Studier, F. W., Rosenberg, A. H., Dunn, J. J., and Dubendorff, J. W. (1990) *Methods. Enzymol. 185*, 60−89.
32. Grubmeyer, C., Segura, E., and Dorfman, R. (1993) *J. Biol. Chem. 268*, 20299−20304.
33. Scapin, G., Sacchettini, J. C., Dessen, A., Bhatia, M., and Grubmeyer, C. (1993) *J. Mol. Biol. 230*, 1304−1308.
34. LeMaster, D. M., and Richards, F. M. (1985) *Biochemistry 24*, 7263−7268.
35. Kao, K., and Michayluk, M. (1975) *Planta 126*, 105−110.
36. Penefsky, H. S. (1977) *J. Biol. Chem. 252*, 2891−2899.
37. Parkin, D. W., Leung, H. B., and Schramm, V. L. (1984) *J. Biol. Chem. 259*, 9411−9417.
38. Xu, Y., Eads, J., Sacchettini, J. C., and Grubmeyer, C. (1997) *Biochemistry 36*, 3700−3712.
39. Kay, L. E., Keifer, P., and Saarinen, T. (1992) *J. Am. Chem. Soc. 114*, 10663−10665.
40. Wishart, D. S., and Sykes, B. D. (1994) *J. Biomol. NMR 4*, 171−180.
41. Delaglio, F., Grzesiek, S., Vuister, G. W., Zhu, G., Pfeifer, J., and Bax, A. (1995) *J. Biomol. NMR 6*, 277−293.
42. Skelton, N. J., Palmer, A. G. I., Akke, M., Kördel, J., Rance, M., and Chazin, W. J. (1993) *J. Magn. Reson., Ser. B 102*, 253−264.
43. Piotto, M., Saudek, M., and Sklenar, V. (1992) *J. Biomol. NMR 2*, 661−665.
44. Fushman, D., Cahill, S., and Cowburn, D. (1997) *J. Mol. Biol. 266*, 173−194.
45. Grzesiek, S., and Bax, A. (1993) *J. Am. Chem. Soc. 115*, 12593−12594.
46. Shaka, A. J., Barker, P. B., and Freeman, R. (1985) *J. Magn. Reson. 64*, 547−552.
47. Eccles, C., Güntert, P., Billeter, M., and Wüthrich, W. (1991) *J. Biomol. NMR 1*, 111−130.
48. Bartels, C., Xia, T.-H., Billeter, M., Güntert, P., and Wüthrich, K. (1995) *J. Biomol. NMR 5*, 1−10.
49. Orekhov, V. Y., Nolde, D. E., Golovanov, A. P., Korzhnev, D. M., and Arseniev, A. S. (1995) *Appl. Magn. Reson. 9*, 581−588.
50. Lipari, G., and Szabo, A. (1982) *J. Am. Chem. Soc. 104*, 4546−4559.
51. Chore, G. M., Szabo, A., Bax, A., Kay, L. E., Driscoll, P. C., and Gronenborn, A. M. (1990) *J. Am. Chem. Soc. 112*, 4989−4991.
52. Mandel, A., Akke, M., and Palmer, A. (1995) *J. Mol. Biol. 246*, 144−163.
53. Kay, L. E., Torchia, D. A., and Bax, A. (1989) *Biochemistry 28*, 8972−8979.
54. Campbell, I. D., Dobson, C. M., Williams, R. J. P., and Wright, P. E. (1973) *FEBS Lett. 57*, 96−99.
55. Forsén, S., and Hoffman, R. A. (1963) *J. Chem. Phys. 39*, 2892−2901.
56. Hyde, E. I., Birdsall, B., Roberts, G. C. K., Feeney, J., and Burgen, A. S. V. (1980) *Biochemistry 19*, 3746−3754.
57. Bain, A. D., and Duns, G. J. (1995) *J. Magn. Reson., Ser. A 112*, 258−260.
58. Bain, A. D., and Duns, G. J. (1996) *Can. J. Chem. 74*, 819−824.
59. Lian, L. Y., and Roberts, G. C. K. (1993) *NMR of Macromolecules: A Practical Approach* (Roberts, G. C. K., Ed.) pp 153−182, Oxford University Press, New York.
60. Jencks, W. P. (1975) *Adv. Enzymol. 43*, 219−410.

BI982057S